Available online at www.sciencedirect.com
ScienceDirect
Journal of Molecular Spectroscopy 239 (2006) 71–87
Journal of MOLECULAR SPECTROSCOPY
www.elsevier.com/locate/jms

Ab initio dipole moment and theoretical rovibrational intensities in the electronic ground state of PH_3

Sergei N. Yurchenko [a], Miguel Carvajal [b], Walter Thiel [a], Per Jensen [c,*]

[a] *Max-Planck-Institut für Kohlenforschung, Kaiser-Wilhelm-Platz 1, D–45470 Mülheim an der Ruhr, Germany*
[b] *Departamento de Fisica Aplicada, Facultad de Ciencias Experimentales, Avenida de las Fuerzas Armadas s/n, Universidad de Huelva, E-21071 Huelva, Spain*
[c] *FB C—Mathematik und Naturwissenschaften, Fachgruppe Chemie, Bergische Universität Wuppertal, D-42097 Wuppertal, Germany*

Received 19 April 2006; in revised form 31 May 2006
Available online 7 June 2006

Abstract

We report a six-dimensional CCSD(T)/aug-cc-pVTZ dipole moment surface for the electronic ground state of PH_3 computed *ab initio* on a large grid of 10 080 molecular geometries. Parameterized, analytical functions are fitted through the *ab initio* data, and the resulting dipole moment functions are used, together with a potential energy function determined by refining an existing *ab initio* surface in fittings to experimental wavenumber data, for simulating absorption spectra of the first three polyads of PH_3, i.e., (ν_2, ν_4), $(\nu_1, \nu_3, 2\nu_2, 2\nu_4, \nu_2 + \nu_4)$, and $(\nu_1 + \nu_2, \nu_3 + \nu_2, \nu_1 + \nu_4, \nu_3 + \nu_4, 2\nu_2 + \nu_4, \nu_2 + 2\nu_4, 3\nu_2, 3\nu_4)$. The resulting theoretical transition moments show excellent agreement with experiment. A line-by-line comparison of the simulated intensities of the ν_2/ν_4 band system with 955 experimental intensity values reported by Brown et al. [L.R. Brown, R.L. Sams, I. Kleiner, C. Cottaz, L. Sagui, J. Mol. Spectrosc. 215 (2002) 178–203] gives an average absolute percentage deviation of 8.7% (and a root-mean-square deviation of 0.94 cm^{-1} for the transition wavenumbers). This is very remarkable since the calculations rely entirely on *ab initio* dipole moment surfaces and do not involve any adjustment of these surfaces to reproduce the experimental intensities. Finally, we predict the line strengths for transitions between so-called cluster levels (near-degenerate levels formed at high rotational excitation) for J up to 60.

Keywords: Phosphine; PH_3; Ab initio dipole moment surfaces; Rovibrational intensities; Energy clusters

1. Introduction

We have recently reported variational calculations of the energies and wavefunctions for highly excited rotational states in the vibrational ground state of phosphine PH_3 [1]. These calculations were based on a potential energy surface for the electronic ground state of PH_3 obtained [2] by refining an existing *ab initio* surface [3] in a simultaneous fitting to *ab initio* data and experimentally derived vibrational energy spacings. At high rotational excitation, the energies form six-fold clusters [1] analogous to the well-known four-fold clusters formed in highly excited rotational states of several triatomic dihydrides H_2X [4,5]. In the present work, we extend the work on PH_3 by computing transition moments of vibrational bands and intensities of individual rotation–vibration transitions. These new calculations are based on a potential energy surface that is a further refinement of that reported in Ref. [2], and on a dipole moment surface (DMS) for the electronic ground state of PH_3 that has been calculated *ab initio* at the CCSD(T)/aug-cc-pVTZ level of theory.

The nuclear-motion calculations of the present work are made by means of our recently developed variational model for the rotation and vibration of an XY_3 molecule [6–9]. The model is based on the Hougen–Bunker–Johns approach [5,10]. We have already applied it to simulate the absorption spectra for selected vibrational bands of NH_3 in its ground electronic state [8,9], employing an *ab initio* DMS calculated at the CCSD(T)/aug-cc-pVTZ level

* Corresponding author. Fax: +49 202 439 2509.
E-mail address: jensen@uni-wuppertal.de (P. Jensen).

0022-2852/$ - see front matter © 2006 Elsevier Inc. All rights reserved.
doi:10.1016/j.jms.2006.06.001

of theory [9]. The theoretical intensity values for NH_3 [8,9] were found to agree very well with the corresponding experimental results. This has encouraged us to perform analogous calculations for PH_3 which we report here. For a detailed description of our model to calculate rotation–vibration energies and intensities for XY_3 molecules, the reader is referred to Refs. [7] and [8].

He et al. [11] have previously computed a partial dipole moment surface for the electronic ground state of PH_3 by density functional theory (DFT); the level of theory was B3LYP/6-311++G(3df,2pd) [12–14]. They considered the dependence of the dipole moment on the internuclear distances in PH_3 only, ignoring the bending motion. The partial DMS was found to produce satisfactory vibrational transition moments for most of the stretching bands whose intensities had been experimentally observed [11]. We validate our newly calculated DMS by comparing the vibrational transition moments and intensities from the present work with the available experimental data. We also compare our transition moments with results of the DFT study by He et al. [11].

The paper is structured as follows: in Section 2 we describe the *ab initio* calculation of the dipole moment surface and the analytical representation of this surface. Section 3 discusses, in a similar manner, the potential energy surface of PH_3 employed in the present work. In Section 4 we give some details of the intensity calculations whose results are reported in the following sections. Section 5 presents the vibrational transition moment values computed with the new *ab initio* DMS; these are compared to the experimental and theoretical values available in the literature. In this section we also present theoretical simulations of the absorption spectra for a number of bands and line strength calculations for transitions between the cluster states mentioned above. Section 6 offers conclusions.

2. The molecular dipole moment

The *ab initio* dipole moment values employed in the present work were computed with the MOLPRO2002 [15,16] package of *ab initio* programs; the calculations were done at the CCSD(T)/aug-cc-pVTZ level of theory (i.e., coupled cluster theory with all single and double substitutions [17] and a perturbative treatment of connected triple excitations [18,19] with the augmented correlation-consistent triple-zeta basis [20,21]) in the frozen-core approximation. Throughout the paper this level of theory will be referred to as ATZfc. Dipole moments were computed using the central finite difference scheme with an added external dipole field of 0.005 a.u. Six calculations were made for each geometry. The convergence thresholds were 10^{-10} for density and 10^{-10} a.u. for energy in Hartree-Fock (HF) calculations, and 10^{-10} a.u. for energy and 10^{-10} for coefficients in CCSD computations.

In the *ab initio* calculations we used a six-dimensional grid consisting of 10080 unique geometries that form a regular grid in the range $1.25\ \text{Å} \leqslant r_1 \leqslant r_2 \leqslant r_3 \leqslant 1.60\ \text{Å}$ and $70° \leqslant \alpha_1, \alpha_2, \alpha_3 \leqslant 110°$. Here, r_i is the instantaneous value of the distance between P and H_i, where H_i is the proton labeled i (= 1,2, or 3); α_i denotes the bond angle $\angle(H_jPH_k)$ where (i,j,k) is a permutation of the numbers (1,2,3).

We utilize the so-called Molecular-Bond (MB) representation [8,9,11,22] to describe the r_i- and α_j-dependence of the electronically averaged dipole moment vector [5,8] $\bar{\boldsymbol{\mu}}$ for PH_3. In the MB representation it is given by

$$\bar{\boldsymbol{\mu}} = \bar{\mu}_1^{\text{Bond}}\mathbf{e_1} + \bar{\mu}_2^{\text{Bond}}\mathbf{e_2} + \bar{\mu}_3^{\text{Bond}}\mathbf{e_3} \tag{1}$$

where the three functions $\bar{\mu}_i^{\text{Bond}}$, $i = 1,2,3$, depend on the vibrational coordinates, and $\mathbf{e}_i$ is the unit vector along the P–H_i bond,

$$\mathbf{e}_i = \frac{\mathbf{r}_i - \mathbf{r}_4}{|\mathbf{r}_i - \mathbf{r}_4|} \tag{2}$$

with $\mathbf{r}_i$ ($i = 1,2,3$) as the position vector of proton i and $\mathbf{r}_4$ as the position vector of the phosphorus nucleus. The representation of $\bar{\boldsymbol{\mu}}$ in Eq. (1) is 'body-fixed' in the sense that it relates the dipole moment vector directly to the instantaneous positions of the nuclei (i.e., to the vectors $\mathbf{r}_i$) [8].

Following Refs. [8,9], we express the three functions $\bar{\mu}_i^{\text{Bond}}$, $i = 1,2,3$, as

$$\bar{\mu}_i^{\text{Bond}} = \sum_{j=1}^{3} (\mathbf{A}^{-1})_{ij} (\bar{\boldsymbol{\mu}} \cdot \mathbf{e}_j) \tag{3}$$

where $(\mathbf{A}^{-1})_{ij}$ is an element of the non-orthogonal 3×3 matrix $\mathbf{A}^{-1}$ obtained as the inverse[1] of

$$\mathbf{A} = \begin{pmatrix} 1 & \cos\alpha_3 & \cos\alpha_2 \\ \cos\alpha_3 & 1 & \cos\alpha_1 \\ \cos\alpha_2 & \cos\alpha_1 & 1 \end{pmatrix}. \tag{4}$$

For symmetry reasons, all three projections can be expressed in terms of a single function $\bar{\mu}_0(r_1, r_2, r_3, \alpha_1, \alpha_2, \alpha_3)$ [8]:

$$\bar{\boldsymbol{\mu}} \cdot \mathbf{e}_1 = \bar{\mu}_0(r_1, r_2, r_3, \alpha_1, \alpha_2, \alpha_3) = \bar{\mu}_0(r_1, r_3, r_2, \alpha_1, \alpha_3, \alpha_2), \tag{5}$$

$$\bar{\boldsymbol{\mu}} \cdot \mathbf{e}_2 = \bar{\mu}_0(r_2, r_3, r_1, \alpha_2, \alpha_3, \alpha_1) = \bar{\mu}_0(r_2, r_1, r_3, \alpha_2, \alpha_1, \alpha_3), \tag{6}$$

$$\bar{\boldsymbol{\mu}} \cdot \mathbf{e}_3 = \bar{\mu}_0(r_3, r_1, r_2, \alpha_3, \alpha_1, \alpha_2) = \bar{\mu}_0(r_3, r_2, r_1, \alpha_3, \alpha_2, \alpha_1), \tag{7}$$

and this function is chosen as an expansion

$$\bar{\mu}_0 = \mu_0^{(0)} + \sum_k \mu_k^{(0)} \xi_k + \sum_{k,l} \mu_{kl}^{(0)} \xi_k \xi_l + \sum_{k,l,m} \mu_{klm}^{(0)} \xi_k \xi_l \xi_m + \sum_{k,l,m,n} \mu_{klmn}^{(0)} \xi_k \xi_l \xi_m \xi_n + \ldots \tag{8}$$

in the variables

$$\xi_k = (r_k - r_e)\exp(-\beta^2 (r_k - r_e)^2), \quad k = 1,2,3, \tag{9}$$

$$\xi_l = \cos(\alpha_{l-3}) - \cos(\alpha_e), \quad l = 4,5,6, \tag{10}$$

where r_e and α_e are the equilibrium values of the bond lengths and bond angles, respectively. We include the fac-

[1] When the molecule is planar, the determinant $|\mathbf{A}| = 0$ and $\mathbf{A}$ cannot be inverted. In this case we set $\bar{\mu}_3^{\text{Bond}} = 0$ in Eq. (1) and express $\bar{\boldsymbol{\mu}}$ in terms of $\mathbf{e}_1$ and $\mathbf{e}_2$ only, i.e., we determine $\bar{\mu}_1^{\text{Bond}}$ and $\bar{\mu}_2^{\text{Bond}}$ in terms of $\bar{\boldsymbol{\mu}} \cdot \mathbf{e}_1$ and $\bar{\boldsymbol{\mu}} \cdot \mathbf{e}_2$.

tor $\exp(-\beta^2(r_k - r_e)^2)$ in Eq. (8) in order to keep the expansion from diverging at large r_k [9,22].

The expansion coefficients $\mu^{(0)}_{k,l,m,\ldots}$ in Eq. (8) are pairwise equal. We have

$$\mu^{(0)}_{k',l',m',\ldots} = \mu^{(0)}_{k,l,m,\ldots} \tag{11}$$

when the indices k', l', m',... are obtained from k, l, m,... by replacing all indices 2 by 3, all indices 3 by 2, all indices 5 by 6, and all indices 6 by 5.

We have determined the values of the expansion parameters in Eq. (8), which we take to fourth order, in a least-squares fitting to the $3 \times 10\,080$ *ab initio* dipole moment projections $\bar{\boldsymbol{\mu}} \cdot \mathbf{e}_j$, $j = 1, 2, 3$, calculated *ab initio* for PH_3 at the ATZfc level of theory. We could usefully vary 108 parameters in the final fitting, which had a root-mean-square (rms) deviation of 0.0008 D. This value can be compared to the typical finite-differences error from the *ab initio* calculations, which was estimated to be less than 0.0001 D. Table 1 lists the optimized parameter values. Parameters, whose absolute values were determined to be less than their standard errors in initial fittings, were constrained to zero in the final fitting and omitted from the table. Furthermore, we give in the tables only one member of each parameter pair related by Eq. (11). We did not observe any improvement of the rms deviation from varying the parameter β. Therefore it was set to 1.0 $Å^{-1}$ and excluded from the fitting.

From the MB representation of the ATZfc dipole moment surface, we calculate the equilibrium dipole

Table 1
ATZfc dipole moment parameters (in D unless otherwise indicated) for the electronic ground state of PH_3 in the Molecular-Bond representation

Parameter	Value	Parameter	Value	Parameter	Value
α_e/deg	93.4	$\mu^{(0)}_{235}$	0.1819(31)[a]	$\mu^{(0)}_{45}$	−0.2268(80)
r_e/Å	1.412	$\mu^{(0)}_{245}$	−0.6207(26)	$\mu^{(0)}_{1456}$	−1.908(16)
β/$Å^{-1}$	1.0	$\mu^{(0)}_{246}$	0.0211(62)	$\mu^{(0)}_{1466}$	−0.3248(63)
$\mu^{(0)}_{0}$	0.332842(12)	$\mu^{(0)}_{255}$	−0.0146(36)	$\mu^{(0)}_{1566}$	−0.4927(70)
$\mu^{(0)}_{1}$	−1.05850(23)	$\mu^{(0)}_{256}$	0.3204(24)	$\mu^{(0)}_{1666}$	−0.4533(45)
$\mu^{(0)}_{3}$	0.13290(12)	$\mu^{(0)}_{266}$	−0.0825(21)	$\mu^{(0)}_{2224}$	−0.206(29)
$\mu^{(0)}_{4}$	0.172867(97)	$\mu^{(0)}_{334}$	−0.2060(16)	$\mu^{(0)}_{2233}$	0.54(10)
$\mu^{(0)}_{5}$	−0.214998(63)	$\mu^{(0)}_{344}$	−0.1301(13)	$\mu^{(0)}_{2244}$	0.0316(97)
$\mu^{(0)}_{11}$	−0.5037(28)	$\mu^{(0)}_{444}$	−0.3432(15)	$\mu^{(0)}_{2245}$	−0.210(16)
$\mu^{(0)}_{13}$	−0.0469(21)	$\mu^{(0)}_{445}$	0.0174(35)	$\mu^{(0)}_{2246}$	−0.031(17)
$\mu^{(0)}_{14}$	−0.1353(15)	$\mu^{(0)}_{456}$	0.0331(15)	$\mu^{(0)}_{2255}$	0.0101(87)
$\mu^{(0)}_{16}$	−0.12622 (100)	$\mu^{(0)}_{466}$	0.08585(63)	$\mu^{(0)}_{2256}$	−0.047(14)
$\mu^{(0)}_{23}$	−0.0501(32)	$\mu^{(0)}_{555}$	0.43471(56)	$\mu^{(0)}_{2333}$	−0.393(64)
$\mu^{(0)}_{33}$	0.0743(13)	$\mu^{(0)}_{556}$	−0.05019(93)	$\mu^{(0)}_{2334}$	−0.096(31)
$\mu^{(0)}_{34}$	−0.17328(87)	$\mu^{(0)}_{1111}$	0.01933(56)	$\mu^{(0)}_{2335}$	−0.245(32)
$\mu^{(0)}_{35}$	−0.0750(11)	$\mu^{(0)}_{1112}$	0.54256(42)	$\mu^{(0)}_{2336}$	0.177(31)
$\mu^{(0)}_{36}$	−0.0146(10)	$\mu^{(0)}_{1115}$	0.15815(47)	$\mu^{(0)}_{2345}$	0.416(14)
$\mu^{(0)}_{44}$	−0.09264(46)	$\mu^{(0)}_{1122}$	−1.026(76)	$\mu^{(0)}_{2444}$	−0.0971(52)
$\mu^{(0)}_{46}$	−0.30957(35)	$\mu^{(0)}_{1123}$	0.177(55)	$\mu^{(0)}_{2445}$	−0.2402(66)
$\mu^{(0)}_{55}$	−0.05508(29)	$\mu^{(0)}_{1124}$	0.226(31)	$\mu^{(0)}_{2455}$	0.1208(62)
$\mu^{(0)}_{56}$	0.05623(53)	$\mu^{(0)}_{1126}$	0.764(59)	$\mu^{(0)}_{2456}$	0.7092(81)
$\mu^{(0)}_{111}$	−0.6994(94)	$\mu^{(0)}_{1136}$	−0.26(12)	$\mu^{(0)}_{2466}$	0.4546(64)
$\mu^{(0)}_{112}$	−0.2531(81)	$\mu^{(0)}_{1144}$	0.284(35)	$\mu^{(0)}_{3335}$	−0.218(27)
$\mu^{(0)}_{114}$	−0.2545(65)	$\mu^{(0)}_{1146}$	−0.381(48)	$\mu^{(0)}_{3445}$	0.1684(61)
$\mu^{(0)}_{115}$	0.4240(38)	$\mu^{(0)}_{1155}$	−0.134(41)	$\mu^{(0)}_{3555}$	0.0822(46)
$\mu^{(0)}_{123}$	−0.186(14)	$\mu^{(0)}_{1156}$	0.078(20)	$\mu^{(0)}_{3556}$	0.3208(52)
$\mu^{(0)}_{124}$	0.1943(58)	$\mu^{(0)}_{1222}$	0.106(19)	$\mu^{(0)}_{3566}$	0.0815(62)
$\mu^{(0)}_{133}$	0.3810(80)	$\mu^{(0)}_{1225}$	−0.252(12)	$\mu^{(0)}_{3666}$	−0.0126(54)
$\mu^{(0)}_{135}$	0.3448(55)	$\mu^{(0)}_{1233}$	0.680(27)	$\mu^{(0)}_{4444}$	−0.1502(28)
$\mu^{(0)}_{136}$	−0.2884(60)	$\mu^{(0)}_{1234}$	−0.173(66)	$\mu^{(0)}_{4445}$	−0.0648(20)
$\mu^{(0)}_{144}$	0.2970(26)	$\mu^{(0)}_{1244}$	0.473(33)	$\mu^{(0)}_{4456}$	−0.2966(34)
$\mu^{(0)}_{146}$	0.2909(24)	$\mu^{(0)}_{1245}$	0.157(74)	$\mu^{(0)}_{4466}$	−0.0240(18)
$\mu^{(0)}_{155}$	0.7612(16)	$\mu^{(0)}_{1246}$	−0.203(55)	$\mu^{(0)}_{4555}$	−0.1158(19)
$\mu^{(0)}_{156}$	0.4363(26)	$\mu^{(0)}_{1256}$	−0.178(16)	$\mu^{(0)}_{4556}$	−0.8468(23)
$\mu^{(0)}_{225}$	0.1819(31)	$\mu^{(0)}_{1335}$	0.183(19)	$\mu^{(0)}_{5566}$	0.0383(25)
$\mu^{(0)}_{226}$	−0.6207(26)	$\mu^{(0)}_{1355}$	0.285(27)	$\mu^{(0)}_{5666}$	0.0041(19)
$\mu^{(0)}_{234}$	0.0211(62)	$\mu^{(0)}_{1444}$	−0.310(22)	$\mu^{(0)}_{6666}$	0.2348(18)

[a] Quantities in parentheses are standard errors in units of the last digit given.

moment as $\mu_e = 0.57736$ D at the experimental equilibrium geometry of $r_1 = r_2 = r_3 = r_e = 1.412$ Å and $\alpha_1 = \alpha_2 = \alpha_3 = \alpha_e = 93.4°$ [23,24]. The experimental value [25] for μ_e is 0.57397(20) D.

3. The potential energy surface

The potential energy surface (PES) for the electronic ground state of PH_3 that we employ in the present work is based on an *ab initio* potential energy surface calculated at the CCSD(T)/aug-cc-pVTZ level of theory by Wang et al. [3]. As described below, we have refined the analytical representation of this surface in an empirical fitting to experimentally derived vibrational term values. The fitting was carried out by means of our variational method for calculating the rotation–vibration energies of an XY_3 molecule directly from the potential energy function; this method is described in Refs. [6,7], to which the reader is referred for details.

In order to ensure a correct description of the PES for a large region of coordinate space, we represent the PES by a Morse-type parameterized expansion (PES type A in Ref. [7])

$$\begin{aligned} V(\xi_1,\xi_2,\xi_3,\xi_{4a},\xi_{4b};\sin\bar{\rho}) &= V_e + V_0(\sin\bar{\rho}) + \sum_j F_j(\sin\bar{\rho})\xi_j + \sum_{j\leqslant k} F_{jk}(\sin\bar{\rho})\xi_j\xi_k \\ &\quad + \sum_{j\leqslant k\leqslant l} F_{jkl}(\sin\bar{\rho})\xi_j\xi_k\xi_l + \sum_{j\leqslant k\leqslant l\leqslant m} F_{jklm}(\sin\bar{\rho})\xi_j\xi_k\xi_l\xi_m \end{aligned} \tag{12}$$

in terms of the stretching variables

$$\xi_k = y_k = 1 - \exp[-a(r_k - r_e)],\ k = 1,2,3, \tag{13}$$

where a is a Morse parameter, the symmetrized bending variables

$$\xi_{4a} = S_{4a} = \tfrac{1}{\sqrt{6}}(2\alpha_1 - \alpha_2 - \alpha_3), \tag{14}$$

$$\xi_{4b} = S_{4b} = \tfrac{1}{\sqrt{2}}(\alpha_2 - \alpha_3) \tag{15}$$

and the variable

$$\sin\bar{\rho} = \tfrac{2}{\sqrt{3}}\sin[(\alpha_1 + \alpha_2 + \alpha_3)/6] \tag{16}$$

for the 'umbrella' motion. The pure inversion potential energy function in Eq. (12) is taken to be

$$V_0(\sin\bar{\rho}) = \sum_{s=1}^{4} f_0^{(s)}(\sin\rho_e - \sin\bar{\rho})^s, \tag{17}$$

and the functions $F_{jk\ldots}(\sin\bar{\rho})$ are defined as

$$F_{jk\ldots}(\sin\bar{\rho}) = \sum_{s=0}^{N} f_{jk\ldots}^{(s)}(\sin\rho_e - \sin\bar{\rho})^s, \tag{18}$$

where $\sin\rho_e$ is the equilibrium value of $\sin\bar{\rho}$ and the quantities $f_0^{(s)}$ and $f_{jk\ldots}^{(s)}$ in Eqs. (17) and (18) are expansion coefficients. The summation limits in Eq. (18) are $N = 3$ for $F_j(\sin\bar{\rho})$, $N = 2$ for $F_{jk}(\sin\bar{\rho})$, $N = 1$ for $F_{jkl}(\sin\bar{\rho})$, $N = 0$ for $F_{jklm}(\sin\bar{\rho})$. In total there are 48 symmetrically unique potential parameters $f_{jk\ldots}^{(s)}$.

In the numerical integration of the inversion Schrödinger equation a grid of 1000 points is used. The size of the vibrational basis set is controlled by the parameter P_{max} defined so that

$$P = 2(v_1 + v_3) + v_2 + v_4 \leqslant P_{max}, \tag{19}$$

where the vibrational quantum numbers v_1, v_3 are associated with the stretching basis functions, v_2 describes the inversion excitation, and v_4 describes the excitation of the small-amplitude bending mode. For the fittings reported here, we use $P_{max} = 10$.

Initial values for the potential parameters $f_{jk\ldots}^{(s)}$ entering into Eqs. (17) and (18) are obtained by analytical transformation of the *ab initio* potential energy function given by Wang et al. [3]. The Morse parameter a is fixed to the value 1.6 $Å^{-1}$ and the structural parameters r_e and α_e are constrained to their experimentally determined equilibrium values [23,24]. The parameters $f_{jk\ldots}^{(s)}$ are then optimized in a fitting to 17 experimentally derived vibrational term values for $^{31}PH_3$; these term values are all below 5000 cm^{-1} (where the energy zero is taken as the energy of the vibrational ground state). In order to prevent the refined PES

Table 2
Refined potential energy parameters (in cm^{-1} unless otherwise indicated) for the electronic ground state of PH_3

Parameter	Value	Parameter	Value
α_e/deg	93.4	$f_{114}^{(1)}$	−23232.82
r_e/Å	1.412	$f_{123}^{(0)}$	644.41
a/Å^{-1}	1.6	$f_{123}^{(1)}$	10658.23
$f_0^{(1)}$	299683.99	$f_{124}^{(0)}$	750.93
$f_0^{(2)}$	−641528.02	$f_{124}^{(1)}$	4762.50
$f_0^{(3)}$	1677731.55	$f_{144}^{(0)}$	−3060.05
$f_1^{(1)}$	−12903.35	$f_{144}^{(1)}$	−9779.15
$f_1^{(2)}$	−550.34	$f_{155}^{(0)}$	−9300.23
$f_1^{(3)}$	−140108.18	$f_{155}^{(1)}$	−9477.98
$f_{11}^{(0)}$	33536.65	$f_{455}^{(0)}$	−7285.22
$f_{11}^{(1)}$	−6271.80	$f_{455}^{(1)}$	−79402.63
$f_{11}^{(2)}$	−57180.28	$f_{1111}^{(0)}$	250.33
$f_{12}^{(0)}$	−70.24	$f_{1112}^{(0)}$	1245.72
$f_{12}^{(1)}$	7170.42	$f_{1114}^{(0)}$	3079.08
$f_{12}^{(2)}$	15098.06	$f_{1122}^{(0)}$	264.23
$f_{14}^{(0)}$	−1546.40	$f_{1123}^{(0)}$	−2504.24
$f_{14}^{(1)}$	−21598.78	$f_{1124}^{(0)}$	−4136.06
$f_{14}^{(2)}$	−73693.30	$f_{1125}^{(0)}$	5440.88
$f_{44}^{(0)}$	18412.02	$f_{1144}^{(0)}$	9759.51
$f_{44}^{(1)}$	42480.94	$f_{1155}^{(0)}$	−5281.46
$f_{44}^{(2)}$	−79403.93	$f_{1244}^{(0)}$	−6595.69
$f_{111}^{(0)}$	−806.09	$f_{1255}^{(0)}$	4089.41
$f_{111}^{(1)}$	−321.59	$f_{1444}^{(0)}$	4948.94
$f_{112}^{(0)}$	−505.03	$f_{1455}^{(0)}$	5736.63
$f_{112}^{(1)}$	766.56	$f_{4444}^{(0)}$	3252.62
$f_{114}^{(0)}$	−52.26		

from attaining an unrealistic shape at geometries much displaced from the equilibrium geometry, we restrained the refined PES to the initial *ab initio* surface by using also the *ab initio* data from Wang et al. [3] as input for the fitting in the manner described in Ref. [2]. For the 17 experimentally derived vibrational term values, we achieved the rms deviation of 1.5 cm^{-1}. For further details of the fitting method, the reader is referred to Ref. [2], where we presented an initial fitting to vibrational term values of PH_3. Owing to improvements in the theoretical model of the present work, relative to that used in Ref. [2], the PES obtained in the present work is more accurate than that reported in Ref. [2]. The most notable improvement is the use of higher-order expansions to represent some terms in the nuclear kinetic energy operator; details are given in Ref. [7]. The optimized potential energy parameter values are compiled in Table 2, while the corresponding, calculated term values are listed in Tables 3 and 4 and compared with the available experimental values. The total rms deviation between theory and experiment for the 28 term values given in Tables 3 and 4 is 1.5 cm^{-1}. The refined surface will be referred to as the ATZfc(R) surface.

We change the vibrational basis set limit P_{max} [Eq. (19)] according to the maximum J value required: for purely vibrational transitions ($J = 0$) we use $P_{max} = 12$; when simulating rotation–vibration absorption spectra ($J < 20$) we use $P_{max} = 8$; and to compute the line strengths of transitions involving highly excited cluster states ($J \leqslant 60$), P_{max} is set to 6. In order to ensure a reasonable accuracy of the vibrational energies in all these simulations, we optimize the PES at a 'compromise' P_{max}-value of 10. In this way we make the fitted parameter values absorb, as much as possible, the deficiencies resulting from the basis set truncation in the least-squares fitting. Thus, the ATZfc(R) parameters are 'effective.' Only when they are used in conjunction with our model for the rotation–vibration motion can we be certain to obtain deviations from experiment around 1.5 cm^{-1} for the energies listed in Tables 3 and 4. On the other hand, the effect of the basis set truncation is found to be less than 2.0 cm^{-1} in the worst case, and so we believe that the ATZfc(R) PES will also provide reasonable accuracy when used with other methods for calculating the rotation–vibration energies and intensities.

Table 3
Band centers $\tilde{\nu}_{fi}$ (in cm^{-1}) and vibrational transition moments μ_{fi} (in D^2) for PH_3: parallel band transitions originating in the vibrational ground state

Band	$\tilde{\nu}_{fi}$		μ_{fi}			
	Obs.[a]	Calc.	Obs.	Ref.[b]	Calc.[c]	Calc.[d]
Rot.[e]			0.57395(30)[f]	[25]		0.5832
ν_2	992.13	992.50	0.08251(5)	[27]		0.0846
$2\nu_2$	1972.55	1972.82	0.00299(5)	[28]		0.0027
$2\nu_4^0$	2226.83[g]	2227.86	0.0176(2)	[28]		0.0055
ν_1	2321.12[g]	2322.04	0.0690[h]	[28]	0.0803	0.0732
$3\nu_2$	2940.77	2940.84				0.0027
$\nu_2 + 2\nu_4^0$	3214.20	3214.37				0.0022
$\nu_2 + \nu_1$	3305.80	3307.72				0.0028
$3\nu_4^3$		3350.28				0.0010
$(\nu_4 + \nu_3)^0$		3463.74				0.0052
$4\nu_2$	3896.02	3895.96				0.0002
$2\nu_2 + 2\nu_4^0$		4187.93				0.0005
$2\nu_2 + \nu_1$	4282.40	4280.71				0.0009
$\nu_2 + 3\nu_4^3$		4333.80				0.0002
$(\nu_2 + \nu_4 + \nu_3)^0$		4443.36				0.0007
$4\nu_4^0$		4435.93				<0.0001
$2\nu_4^0 + \nu_1$		4515.98				0.0007
$(2\nu_4^2 + \nu_3)^0$		4557.13				0.0003
$2\nu_1$	4566.26	4563.28			0.0034	0.0045
$2\nu_3$	4644.66	4644.90			0.0011	0.0012
$2\nu_2 + 2\nu_1$	6503.10	6498.88				0.0001
$3\nu_1$	6714.60	6708.91			0.0001	0.0003
$\nu_1 + 2\nu_3$	6881.53	6876.84			0.0004	0.0002
$3\nu_3^3$	6971.16	6876.84			0.0001	0.0001
$2\nu_1 + \nu_3 + \nu_4$	7775.50	7775.78				<0.0001
$\nu_1 + 2\nu_3 + \nu_4$	7961.90	7967.69				<0.0001

[a] See Ref. [3] for original references unless otherwise indicated.
[b] Reference for the observed μ_{fi} value given under the heading 'Obs.'
[c] Calculated from the dipole moment surface of Ref. [11] (MB representation).
[d] Calculated from the dipole moment surface reported in the present work.
[e] Rotational spectrum.
[f] Experimental uncertainties are given in parentheses (in units of the last digit quoted) where available.
[g] Ref. [28].
[h] Tentative estimate from Ref. [28].

Table 4
Band centers $\tilde{\nu}_{fi}$ (in cm^{-1}) and vibrational transition moments μ_{fi} (in D^2) for PH_3: perpendicular band transitions originating in the vibrational ground state

Band	$\tilde{\nu}_{fi}$		μ_{fi}			
	Obs.[a]	Calc.	Obs.	Ref.[b]	Calc.[c]	Calc.[d]
ν_4	1118.31	1117.87	0.08626(5)[e]	[27]		0.0865
$\nu_2+\nu_4$	2108.15[f]	2107.17	0.01102(6)	[28]		0.0093
$2\nu_4^2$	2234.93[f]	2234.57	0.0176(2)	[28]		0.0015
ν_3	2326.87[f]	2329.18	0.130[g]	[28]	0.1437	0.1389
$2\nu_2+\nu_4$		3083.97				0.0013
$\nu_2+2\nu_4^2$		3220.90				0.0010
$\nu_2+\nu_3$		3311.61				0.0011
$3\nu_4^1$		3336.32				0.0015
$\nu_4+\nu_1$	3423.90	3423.05				0.0102
$(\nu_4+\nu_3)^1$		3444.17				0.0023
$3\nu_2+\nu_4$		4048.23				<0.0001
$2\nu_2+2\nu_4^2$		4194.36				0.0001
$2\nu_2+\nu_3$		4282.33				0.0013
$\nu_2+3\nu_4^1$		4320.23				<0.0001
$\nu_2+\nu_4+\nu_1$		4404.13				0.0014
$\nu_2+\nu_4+\nu_3$		4424.83				0.0007
$4\nu_4^2$		4443.02				0.0001
$4\nu_4^4$		4464.38				0.0001
$2\nu_4^0+\nu_3$		4504.03				0.0004
$2\nu_4^2+\nu_1$		4535.92				0.0002
$\nu_1+\nu_3$	4565.78	4561.85			0.0047	0.0066
$2\nu_3$		4655.27				0.0047
$2\nu_4^2+\nu_3$		4535.92				0.0002
$\nu_2+2\nu_3^2$	5540.00	5535.38				0.0016
$\nu_4+2\nu_1$	5645.40	5634.14				0.0018
$3\nu_3^1$	6714.60	6708.95			0.0004	0.0004
$2\nu_1+\nu_3$	6883.73	6882.83			0.0001	0.0002
$\nu_1+2\nu_3^2$	6890.86	6892.64			0.0003	0.0002
$\nu_2+3\nu_3^1$	7679.10	7675.37				0.0003
$\nu_4+3\nu_1$	7775.50	7774.52				0.0001
$\nu_4+2\nu_1+\nu_3$	7961.90	7959.08				0.0001

[a] See Ref. [3] for original references unless otherwise indicated.
[b] Reference for the observed μ_{fi} value given under the heading 'Obs.'
[c] Calculated from the dipole moment surface of Ref. [11] (MB representation).
[d] Calculated from the dipole moment surface reported in the present work.
[e] Experimental uncertainties are given in parentheses (in units of the last digit quoted) where available.
[f] Ref. [28].
[g] Tentative estimate from Ref. [28].

4. Intensity calculations

We aim at calculating intensities of electric dipole transitions within the ground electronic state of PH_3. We neglect hyperfine structure (i.e., the effect of the nuclear spins on the molecular energies). In this approximation, the line strength of an individual rotation–vibration transition (from an initial state i with rotation–vibration wavefunction $|\Phi_{rv}^{(i)}\rangle$ to a final state f with rotation–vibration wavefunction $|\Phi_{rv}^{(f)}\rangle$) within an isolated electronic state of an XY_3 pyramidal molecule is given by Eq. (21) of Ref. [8]. This expression is used in the intensity calculations reported in the present work. The rotation–vibration wavefunctions $|\Phi_{rv}^{(i)}\rangle$ and $|\Phi_{rv}^{(f)}\rangle$ are obtained, together with the associated rotation–vibration energies, in variational calculations with the theoretical model for describing the rotation and vibration of an XY_3 molecule [6,7] that we have already discussed in the preceding sections. The extension of the model to the computation of intensities is discussed in Refs. [8,9]. When simulating absorption spectra, we calculate for each rotation–vibration line the integral of the absorption cofficient $\epsilon(\tilde{\nu})$ (which depends on the absorption wavenumber $\tilde{\nu}$) over the line; this quantity is proportional to the line strength and given by Eq. (6) of Ref. [8].

In addition to calculating the line strengths of individual rotation–vibration transitions, we also compute vibrational transition moments defined as

$$\mu_{fi} = \sqrt{\sum_{\alpha=x,y,z} |\langle \Phi_{vib}^{(f)} \mid \bar{\mu}_\alpha \mid \Phi_{vib}^{(i)} \rangle|^2}, \tag{20}$$

where $|\Phi_{vib}^{(w)}\rangle$, $w = i$ or f, are vibrational wavefunctions describing states with $J = 0$. In the absence of strong Coriolis-type resonances, these transition moments determine the intensities of entire vibrational bands (see, for example, Ref. [26]). The matrix elements required in Eq. (20) are gen-

erated by techniques described in Ref. [7] for matrix elements of the potential energy function.

5. Applications

5.1. Transition moments

We have calculated the vibrational transition moments [Eq. (20)] for selected vibrational bands of PH_3. The calculation is based on the refined ATZfc(R) PES and the *ab initio* DMS described in Section 2. The variational calculations to determine the rotation–vibration energies and wavefunctions are made as described in Section 3 with $P_{\max} = 12$ [Eq. (19)]. The results are included in Tables 3 and 4.

By comparing our theoretical values for the vibrational transition moments for PH_3 to experimental values and theoretical values from the literature [11] we can assess the quality of the ATZfc dipole moment surface. We make this comparison in Tables 3 and 4. It is seen that the ATZfc DMS provides a reasonable description of the intensities of bands involving excitation of both stretching and bending modes. This is especially valuable for the simulations of spectra with transitions to highly excited vibrational states, for which strong interactions prevail. The relative deviation between experiment and theory is 1.6% for the 'permanent dipole moment' (the expectation value of the dipole moment in the vibrational ground state). For transition moments of the fundamental bands ν_1, ν_2, ν_3, and ν_4, the deviations are 6.1%, 2.5%, 6.9%, and 0.3%, respectively. The agreement is seen to be better for the two bending bands ν_2 and ν_4. Our relative deviation for the stretching bands ν_1 and ν_3 is in accordance with the experimental accuracy, which was estimated to be larger than 10% [28].

5.2. Simulations of spectra

We report simulations of PH_3 absorption bands in three wavenumber regions: a region at 9 μm with transitions from the vibrational ground state to the state 'dyad' (ν_2,ν_4); a region at 5 μm with transitions to the 'pentad' $(2\nu_2, \nu_2+\nu_4, 2\nu_4, \nu_1, \nu_3)$; and a region at 3 μm with transitions to the manifold of states $(3\nu_2, 2\nu_2+\nu_4, \nu_2+2\nu_4, \nu_1+\nu_2, \nu_3+\nu_2, 3\nu_4, \nu_1+\nu_4, \nu_3+\nu_4)$. The simulated bands contain rovibrational transitions between states with $J<20$ and with the vibrational ground state as lower vibrational state. The term values of the upper states involved in the transitions are plotted in Fig. 1 as reduced energies $E_{v,Jk} - E^{\max}_{v=0,Jk}$ against the angular momentum quantum number J. Here v is a short-hand notation for (v_1,v_2,v_3,v_4), $v=0$ stands for the ground vibrational state, and $E^{\max}_{v=0,Jk}$ is the maximum energy for the J multiplet in question in the vibrational ground state. Variationally computed eigenfunctions (and eigenvalues) are labeled by the quantum numbers $\{v,J,k\}$, obtained from the basis function with the largest contribution to the wavefunction for the state in question.

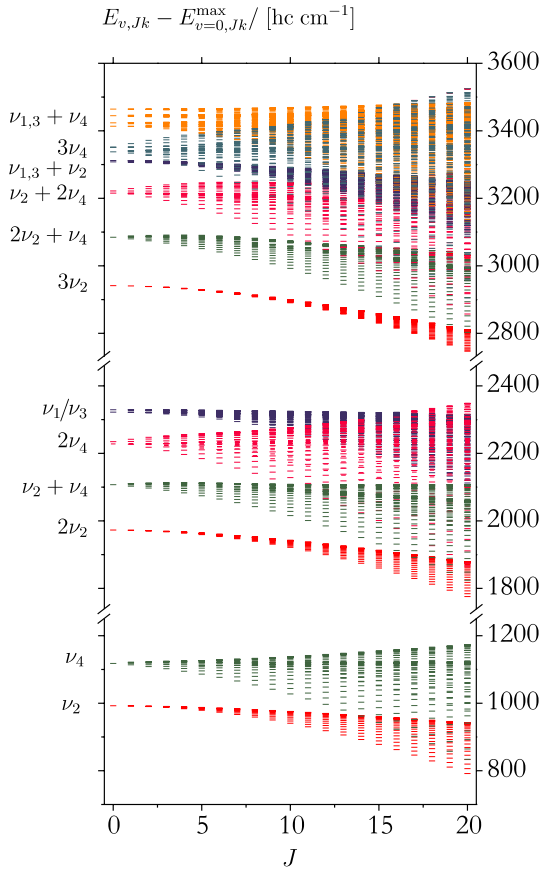

Fig. 1. Variationally computed, reduced rovibrational term values $E_{v,Jk} - E^{\max}_{v=0,Jk}$ (see text), plotted against the angular momentum quantum number J for the 1st, 2nd, and 3rd polyads of PH_3.

The term values in Fig. 1 exhibit a distinct polyad structure. In these polyads, there is often significant interaction between the individual rovibrational states, and this makes our $\{v,J,k\}$ labeling ambiguous in many cases. Since the corresponding experimental assignment is ambiguous in a similar manner, the correlation between the theoretical and the experimental spectra is not always straightforward.

The simulated spectra are drawn as stick diagrams in Figs. 2–4. The height of the stick representing a line is the integrated absorption coefficient computed from Eq. (6) of Ref. [8]. The line strengths are computed with the spin statistical weight factors $g_{\rm ns} = 8,8,8$, respectively, for the A_1, A_2, and E symmetry levels. The simulations are made with the ATZfc(R) potential energy surface and the ATZfc dipole moment surface. As mentioned above, in order to reduce the sizes of the matrices to be diagonalized and thus make the calculations feasible, the vibrational basis set has $P_{\max} = 8$ [Eq. (19)]. Even with this reduction the computed rovibrational wavefunctions consist of thousands of expansion terms. These wavefunctions are then used to calculate the matrix elements required in Eq. (20). In order to facilitate this process we apply a prescreening procedure to truncate the wavefunction expansions: all terms with contribution less than a given threshold are cut off and excluded from the integration. We found

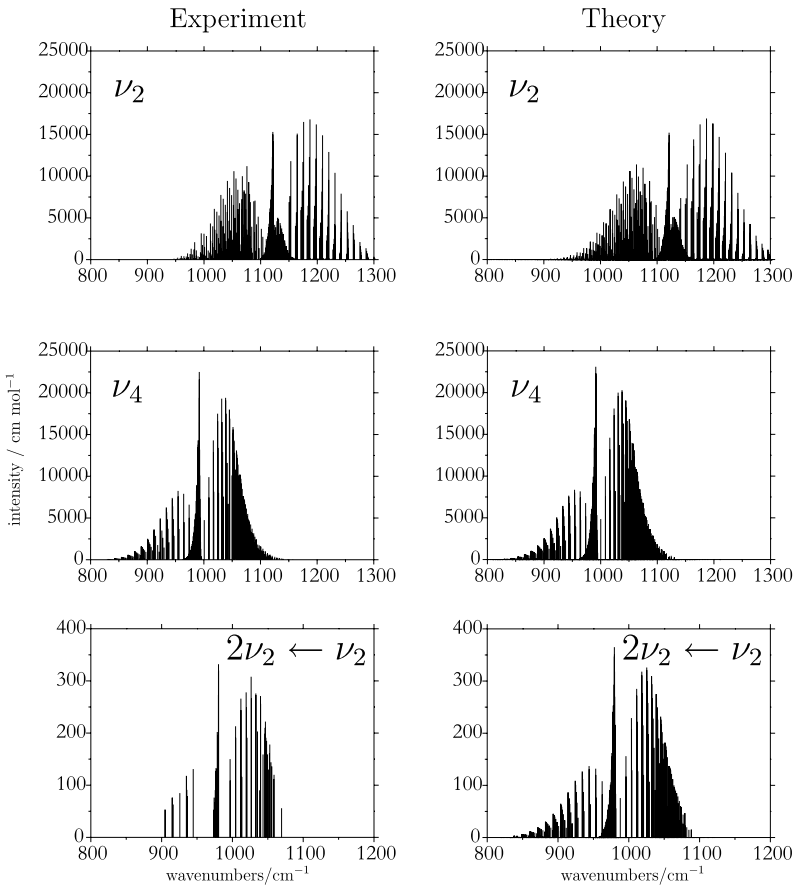

Fig. 2. Comparison of simulated and observed [27] spectra near 9 μm: the v_2, v_4, and $2v_2 \leftarrow v_2$ absorption bands of PH_3.

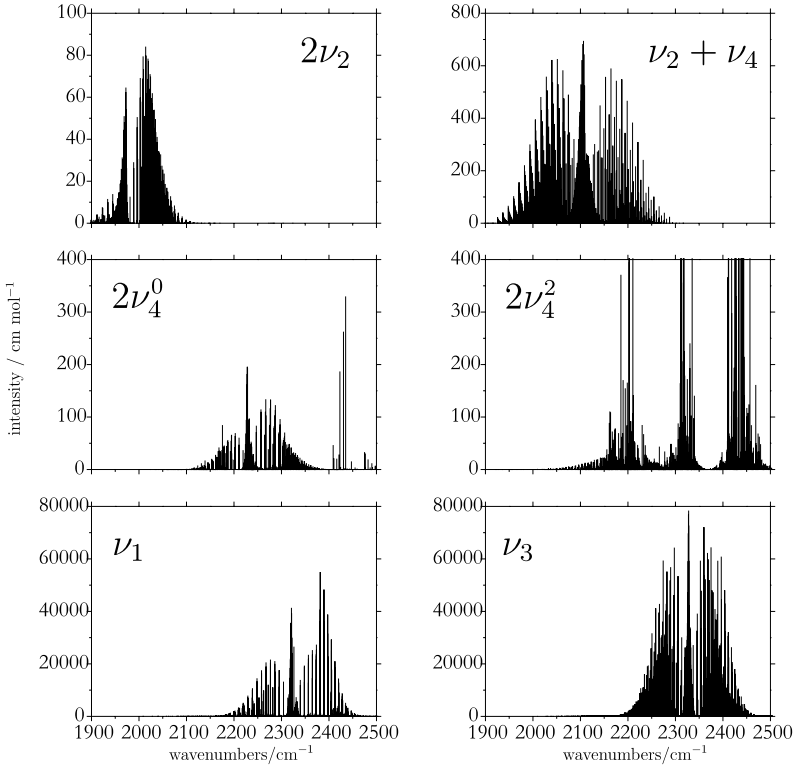

Fig. 3. Simulated spectra near 5 μm: the v_1, v_3, $2v_4^0$, $2v_4^2$, $v_2 + v_4$, and $2v_2$ absorption bands of PH_3.

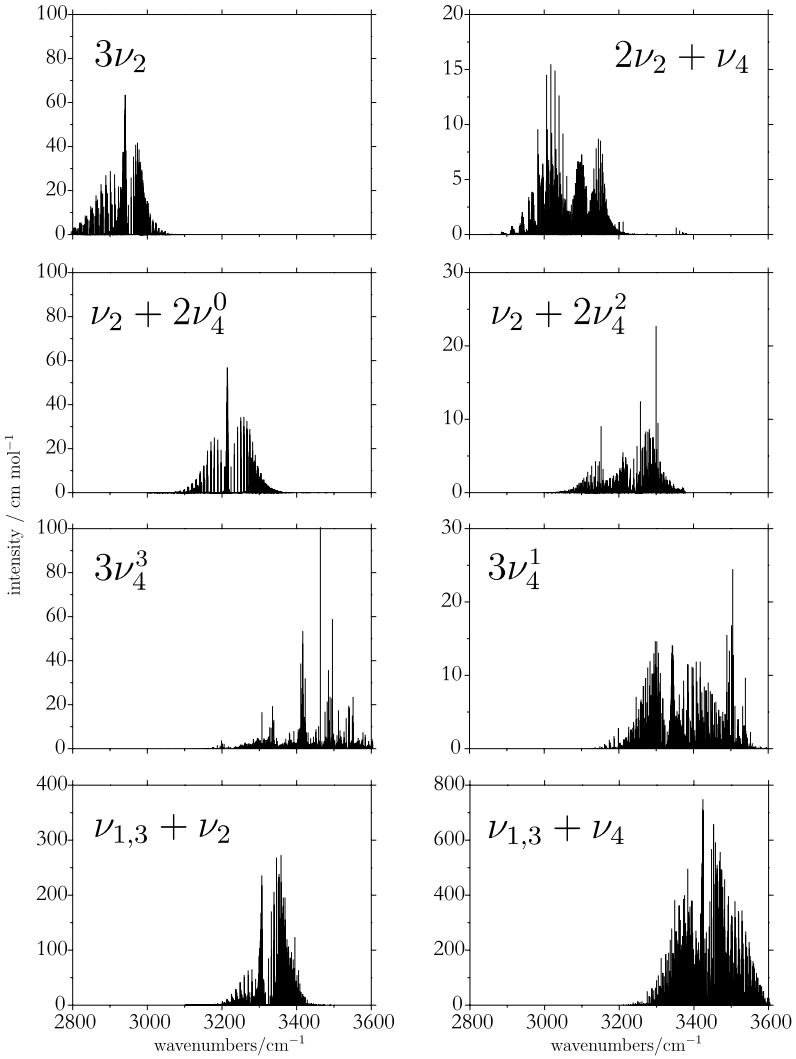

Fig. 4. Simulated spectra near 3 μm: the $v_1 + v_4$, $v_3 + v_4$, $v_1 + v_2$, $v_3 + v_2$, $v_2 + 2v_4^0$, $v_2 + 2v_4^2$, $2v_2 + v_4$, $3v_2$, $3v_4^1$, and $3v_4^3$ absorption bands of PH_3.

that the threshold of 10^{-8} represents an appropriate compromise between the accuracy and the computation time.

We compare the theoretical intensities for PH_3 with experimental data from the recent spectroscopic study of the fundamental transitions to the v_2/v_4 dyad by Brown et al. [27]. In addition, Brown et al. [27] observed 64 transitions in the $2v_2 \leftarrow v_2$ hot band, and so we also simulate this hot band. Our simulations are done with $T = 300$ K as the experimental spectra for the v_2/v_4 and the $2v_2 \leftarrow v_2$ bands [27] have been recorded at room temperature. In computing the integrated absorption coefficient, we use the partition function value $Q = 4943.75$; this value is obtained at $T = 300$ K from the variationally calculated term values with $J < 20$, $v_1 \leqslant 2$, $v_2 \leqslant 6$, $v_3 \leqslant 2$, and $v_4 \leqslant 4$. We discard transitions for which the calculated value of the integrated absorption coefficient (Eq. (6) of Ref. [8]) is less than 10^{-8} cm mol^{-1}.

In Fig. 2 we show simulations of the v_2, v_4, and $2v_2 \leftarrow v_2$ absorption bands of PH_3. The bands are artificially separated according to the assignment of the upper state. Each simulated band is compared to an 'experimentally derived' stick spectrum drawn with experimental values for transition wavenumbers and intensities [27]; these transitions are also artificially separated according to the 'experimental' assignment of the upper state. The experimentally derived spectra show only the transitions assigned in Ref. [27] and this explains why the experimental spectra generally contain less lines than the simulated ones. In the simulated and the experimentally derived stick spectra, the intensities are given as integrated absorption coefficients (Eq. (6) of Ref. [8]) in cm mol^{-1}. The experimental values, originally [27] given in cm^{-2} atm^{-1}, were converted to cm mol^{-1} at $T = 300$ K. Note that the same absolute intensity scale is used for the two members of each theoretical/experimental spectrum pair. For the v_2/v_4 and $2v_2 \leftarrow v_2$ bands in Fig. 2, there is remarkable agreement between the simulated and experimentally derived stick spectra. These results are in keeping with the close agreement between experiment and theory for the corresponding transition moment values in Tables 3 and 4. The calculated value of 0.1152 D for the $2v_2 \leftarrow v_2$ transition moment also agrees well with its experimental counterpart of 0.1177(4) D from Ref. [27].

In order to get a more quantitative measure of the accuracy of our intensity simulations, we have performed a line-by-line comparison between theoretical and experimental spectra. Brown et al. [27] have assigned a total of 979 lines in the experimental ν_2/ν_4 spectrum. For the detailed line-by-line comparison we had to establish a one-to-one correspondence between the experimental and theoretical assignments. For 955 of the 979 lines, the quantum numbers assigned by Brown et al. [27] were identical to those assigned by our program from the basis functions with the largest contributions to the wavefunctions of the states involved in the transition. The remaining 24 lines could not be unambiguously related to the theoretical transitions and were excluded from the line-by-line analysis. This involved 10 relatively strong lines (with intensities between 1300 and 7000 $\mathrm{cm\,mol^{-1}}$), and 14 rather weak lines (with intensities $<500\ \mathrm{cm\,mol^{-1}}$). Apart from these lines, there were also a number of cases in which one experimental transition corresponded to two theoretical ones; these transitions involve A_1/A_2 level pairs that are effectively degenerate at low J. In such cases we included both theoretical intensity values in our analysis. In this way we ended up with 955 experimental transitions corresponding to 1138 theoretical intensity values, for which we obtain an average absolute percentage deviation between theoretical and experimental intensity values, defined as

$$\Delta_{\%} = 100 \times \frac{1}{N_{\mathrm{lin}}} \sum_{i=1}^{N_{\mathrm{lin}}} \frac{|\, I^{(i)}_{\mathrm{obs}} - I^{(i)}_{\mathrm{calc}} \,|}{I^{(i)}_{\mathrm{obs}}} = 8.7\%, \tag{21}$$

where $N_{\mathrm{lin}} = 1138$ is the number of transitions compared, and $I^{(i)}_{\mathrm{obs}}$ and $I^{(i)}_{\mathrm{calc}}$ are the observed and calculated intensities, respectively, of transition i. The transition wavenumbers have a root-mean-square deviation of $0.94\ \mathrm{cm^{-1}}$ for the 1138 transitions. The theoretical results are computed with a purely *ab initio* dipole moment function; no fitting of dipole moment parameters to experimental intensities has been made. Brown et al. [27] have carried out such a fitting to the observed ν_2 and ν_4 intensities and obtained intensity deviations of 1.5% and 2.1%, respectively. The 'pure' *ab initio* deviation of 8.7% that we achieve here is of course larger than the 'optimized' values, but not enormously so.

In Figs. 3 and 4 we show simulations of the absorption bands from the second and third polyads of PH_3, which make up the 5 μm and 3 μm regions, respectively. The bands ν_1/ν_3 are much more intense than the other members of these systems; this agrees with the transition moments from Tables 3 and 4.

Because of the ambiguity of the assignment at high J mentioned above, some of the bands shown in Figs. 3 and 4 might contain transitions that do not belong to them. For example, three unusually strong branches appearing in the $2\nu_4^2$ band (Fig. 3) probably borrow intensity from the ν_1/ν_3 bands. Indeed, according to the vibrational transition moments from Tables 3 and 4, the intensities from the $2\nu_4^0$ and $2\nu_4^2$ transitions must be on the order of $200\ \mathrm{cm\,mol^{-1}}$ and $50\ \mathrm{cm\,mol^{-1}}$, respectively.

The weakest bands that we consider correspond to vibrational transition moments on the order of magnitude of 0.001 D, to avoid uncertainties related to numerical issues (fitting accuracy, etc.).

5.3. Transitions between cluster states at high J

As mentioned in Section 1, we have recently shown [1] that in the vibrational ground state of PH_3, the highly excited rotational states form clusters. There are two types of energy clusters found theoretically in the vibrational ground state of PH_3: two-fold and six-fold clusters. The two-fold clusters are formed by the two energy levels characterized by the largest value of $K_c = |k_c| = J$ [5,26], where k_c is the projection, in units of ħ, of the total angular momentum onto the z axis, which coincides with the C_3 axis [26] for a PH_3 molecule in its equilibrium configuration (see Fig. 5). These levels have the lowest energies in each J multiplet, and the two-fold clusters are the 'usual' $k_c = \pm J$ clusters found for an oblate symmetric top at high J. More unusually, the highest four rotational term values in each J multiplet form a six-fold cluster whose wavefunction components span the six-dimensional representation

$$A_1 \oplus A_2 \oplus 2E \tag{22}$$

of the molecular symmetry group $\mathbf{C}_{3v}(M)$ [5,26]. The states at highest and lowest energy in each cluster span the $A_1 \oplus A_2$ representation, whereby the state at highest energy has $A_1(A_2)$ symmetry for J even(odd), while each of the two 'inner' energy levels belongs to the E symmetry representation so that these two energy levels are doubly degenerate.

The rotational level clustering for the ground vibrational state of PH_3 is illustrated in Fig. 6, where we plot the difference $E_{v=0,Jk} - E^{\max}_{v=0,Jk}$ as a function of J; $E^{\max}_{v=0,Jk}$ is here the maximum energy for the J multiplet in question. The energies are calculated from the ATZfc(R) potential energy surface as described in Section 4; the basis set used has $P_{\max} = 6$ [Eq. (19)].

As J increases, the *first* six-fold cluster in the vibrational ground state of PH_3 forms at the top of the J manifold at $J \approx 35$ (see Ref. [1]); we also sometimes refer to this cluster as the 'top' one. The levels in the first cluster are shown as

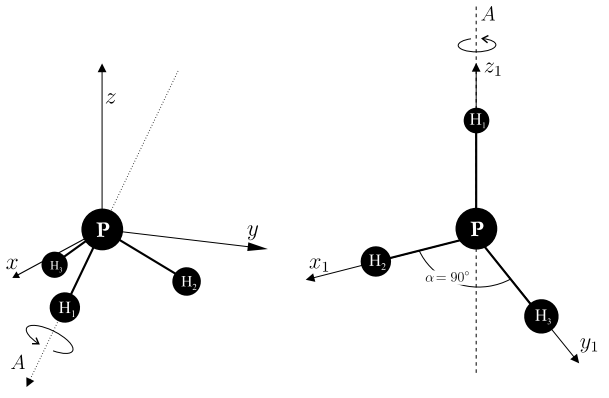

Fig. 5. The molecule-fixed axis systems xyz and $x_1y_1z_1$ of PH_3.

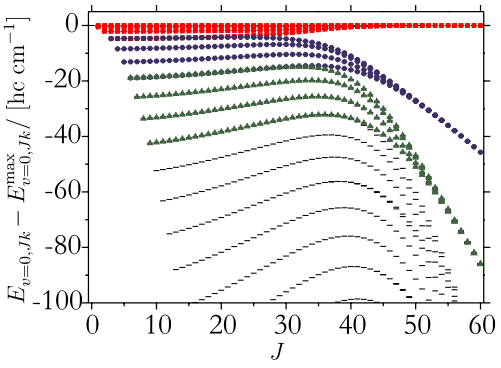

Fig. 6. Reduced rotational term values ($E_{v=0,Jk} - E^{max}_{v=0,Jk}$) in the vibrational ground state of PH_3. The levels belonging to the first, second, and third six-fold clusters are indicated by squares, circles, and triangles, respectively.

squares in the term value diagram of Fig. 6. As J increases, more clusters form below the first one. We call these the *second*, *third*, ... clusters, counted in order of descending energy. Table 5 gives the term values of the states in the first, second, and third clusters for selected J values. In all six-fold clusters, the six cluster states span the representation of $\mathbf{C}_{3v}(M)$ given in Eq. (22).

A detailed analysis of the cluster states has been given in Ref. [1]. In the present work, we report calculations of the line strength values for transitions connecting different cluster states. At equilibrium, PH_3 is an oblate rigid rotor [5] so that in rigid-rotor notation, the four highest energy levels at a given J value (i.e., the four energy levels making up the first cluster) have $K_c = 0, 1, 2, 3$, respectively, when the energies are considered in descending order; the four levels making up the second cluster have $K_c = 3, 4, 5, 6$, respectively, and so on for the following clusters. We use the standard notation $K_c = |k_c|$, where the signed quantum number k_c ($-J \leqslant k_c \leqslant J$) is defined in Ref. [5]. For PH_3, rotation–vibration transitions obey the general selection rules [5,26]

$$A_1 \leftrightarrow A_2 \quad \text{and} \quad E \leftrightarrow E. \tag{23}$$

It can be shown [5] that as a consequence of this, in the vibrational ground state of PH_3 only rotational transitions with $\Delta k_c = 3t$, where t is an integer, have non-vanishing intensity.

Fig. 7 illustrates the 'cluster' transitions that we consider in the present work. In Fig. 7(A) we show the so-called intra-cluster transitions, i.e., the $\Delta J = 0$ transitions within a given cluster. Two kinds of these satisfy Eq. (23): an $A_1 \leftrightarrow A_2$ transition connects the lowest level of the cluster with the highest one, and an $E \leftrightarrow E$ transition connects the two 'inner' levels. In the first cluster, the $A_1 \leftrightarrow A_2$ transition corresponds to $k_c = 0 \leftarrow \pm 3$, and the $E \leftrightarrow E$ transition corresponds to $k_c = \pm 1 \leftarrow \mp 2$ where the signs are correlated. Consequently, both of these transitions are $\Delta k_c = \pm 3$ transitions.

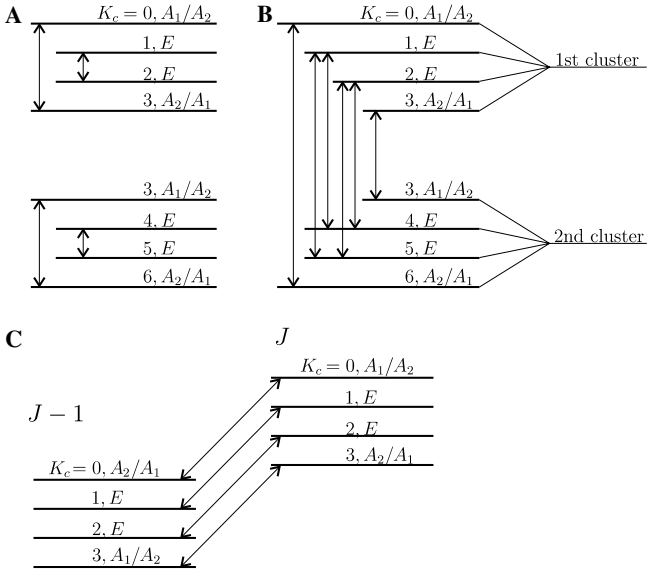

Fig. 7. A schematic diagram defining the (A) intra-cluster $\Delta J = 0$ transitions; (B) inter-cluster $\Delta J = 0$ transitions; (C) inter-cluster $\Delta J = 1$ transitions.

Table 5
Vibrational ground state term values (in cm^{-1}) of PH_3 for the first three clusters

Cluster	$J = 10$	$J = 20$	$J = 30$	$J = 40$	$J = 50$	$J = 59$	$J = 60$
1	487.2787	1844.3921	4029.7576	6989.6079	10673.5757	14565.7292	15030.1538
	486.7691	1843.9288	4029.3693	6989.4834	10673.5724	14565.7292	15030.1538
	485.2388	1842.5376	4028.2417	6989.2122	10673.5660	14565.7292	15030.1538
	482.6845	1840.3092	4027.0279	6989.0631	10673.5628	14565.7291	15030.1538
2	482.6811	1840.1135	4024.9472	6978.6103	10646.6220	14522.0281	14984.4766
	479.0930	1836.9455	4022.9145	6977.8169	10646.5218	14522.0263	14984.4755
	474.4578	1832.7326	4019.3289	6975.6890	10646.3141	14522.0227	14984.4733
	468.7625	1827.5572	4014.9076	6973.6101	10646.2061	14522.0209	14984.4723
3	468.7625	1827.5562	4014.7715	6970.1422	10626.6905	14483.7848	14944.2363
	461.9886	1821.4024	4009.4842	6967.1125	10625.9281	14483.7409	14944.2081
	454.1146	1814.2508	4003.2602	6962.0323	10624.0118	14483.6521	14944.1513
	445.1151	1806.0799	3996.1546	6956.2033	10622.6354	14483.6072	14944.1227

Fig. 7(B) defines the $\Delta J = 0$ inter-cluster absorption transitions starting in the second cluster and ending in the first cluster. There are two $A_1 \leftrightarrow A_2$ transitions of this type. One starts in the top state of the second cluster and ends in the bottom state of the first cluster. Both of these states have $K_c = 3$ in rigid-rotor notation, and so the corresponding transition has $\Delta k_c = 0$. The other $A_1 \leftrightarrow A_2$ transition connects the bottom state of the second cluster with the top state of the first cluster; it obviously has $\Delta k_c = \pm 6$. There are four $E \leftrightarrow E$ transitions between the two adjacent clusters. In the first cluster, the two E states have $K_c = 1$ and 2, respectively, while the corresponding E states for the second cluster have $K_c = 4$ and 5, respectively. Thus, of the four $E \leftrightarrow E$ inter-cluster transitions two correspond to $k_c = \pm 1 \leftarrow \pm 4$ and $k_c = \pm 2 \leftarrow \pm 5$, respectively, and have $\Delta k_c = \pm 3$. The other two correspond to $k_c = \pm 1 \leftarrow \mp 5$ and $k_c = \pm 2 \leftarrow \mp 4$, respectively, and have $\Delta k_c = \pm 6$.

Finally, in Fig. 7(C) we show the $\Delta J = 1$ transitions connecting the first cluster at $J - 1$ with that at J. In each of the two clusters, the energy levels have $K_c = 0, 1, 2, 3$, respectively, and the dominant inter-cluster transitions have $\Delta k_c = 0$; we have four such transitions with $k_c = 0 \leftarrow 0$, $\pm 1 \leftarrow \pm 1$, $\pm 2 \leftarrow \pm 2$, and $\pm 3 \leftarrow \pm 3$, respectively. The $k_c = 0 \leftarrow 0$ and $\pm 3 \leftarrow \pm 3$ transitions are $A_1 \leftrightarrow A_2$ (the A_1/A_2 symmetry label of the top and bottom cluster state alternates with the parity of J), and the two other transitions are $E \leftrightarrow E$. In principle, there are two further $E \leftrightarrow E$ transitions with $k_c = \pm 1 \leftarrow \mp 2$ and $k_c = \pm 2 \leftarrow \mp 1$, respectively (i.e., with $\Delta k_c = \pm 3$), analogous to the $E \leftrightarrow E$ transitions in Fig. 7(A). However we neglect these in Fig. 7(C) since they are very weak in comparison with the $\Delta k_c = 0$ transitions (see, for example, Refs. [5,26]).

In the present work, we compute the transition wavenumbers and line strengths of the transitions defined in Fig. 7 numerically by variational methods. The line strengths are calculated from Eq. (21) of Ref. [8]. In order to understand the numerical results, however, it is useful to consider also the customary approach to molecular rotation–vibration theory (see Ref. [29] or the review articles [30,31]). To calculate spectra in the customary approach, we solve the rotation–vibration Schrödinger equation by diagonalizing the matrix representation of the rotation–vibration Hamiltonian $\hat{H}_{rv}$ set up in a harmonic-oscillator/rigid-rotor basis. The diagonalization is carried out by means of successive contact transformations [29–31]. The contact transformation method is based on perturbation theory, it leads to a Hamiltonian that can be directly related to the models used for interpreting experimental spectra.

The line strengths of rotational and rotation–vibration transitions depend on the dipole moment components $\bar{\mu}_A$, $A = X, Y, Z$, along the space-fixed (or laboratory-fixed) axes XYZ [5,29]. To obtain rovibrational line strengths in the contact-transformation scheme, we first express the space-fixed dipole moment components $\bar{\mu}_A$ in terms of the components (μ_x, μ_y, μ_z) along the molecule-fixed axes xyz. This axis system is chosen such that it follows the rotational motion of the molecule; for details see, for example, Refs. [5,29,31]. We have

$$\bar{\mu}_A = \sum_{\alpha=x,y,z} \lambda_{\alpha A} \bar{\mu}_\alpha, \tag{24}$$

where the $\lambda_{\alpha A}$ are direction cosines (see, for example, [5]) effecting the transformation between the xyz and XYZ axis systems. The quantity $\bar{\mu}_\alpha$ depends on the nuclear coordinates. It can be expressed as a Taylor expansion in the normal coordinates of the molecule.

We now introduce the effective dipole moment operator

$$\tilde{\mu}_A = e^{i\hat{S}} \left(\sum_{\alpha=x,y,z} \lambda_{\alpha A} \bar{\mu}_\alpha \right) e^{-i\hat{S}}, \tag{25}$$

which is obtained from the 'untransformed' dipole moment operator by the same contact transformation that was applied to the rotation–vibration Hamiltonian $\hat{H}_{rv}$ in order to obtain an effective rotational Hamiltonian, the so-called Watsonian $\tilde{H}_{rv}$ [29]. Here, $\hat{S}$ is a Hermitian operator that effects the contact transformation on $\hat{H}_{rv}$. The resulting effective operator $\tilde{\mu}_A$, and its matrix elements between harmonic-oscillator/rigid-rotor basis functions (which determine the rovibrational line strengths), have a very complex form, especially at high order of the expansion. The values of the constant expansion coefficients in $\tilde{\mu}_A$ can be obtained by fitting to experimentally determined line strengths, just as the parameter values in the Watsonian $\tilde{H}_{rv}$ are determined in fittings to experimentally derived energy differences.

For C_{3v} molecules, intensity expressions have been obtained in the customary approach by Tarrago et al. [32]. We will use these expressions to explain qualitatively the main features of the cluster transitions in Fig. 7.

In Fig. 8 we plot against J the transition wavenumbers and line strengths, respectively, of the $\Delta J = 0$ intra-cluster transitions defined in Fig. 7(A) for the first, second, and third clusters formed in the vibrational ground state of PH_3. As the clusters form for high J, the wavenumbers of all the intra-cluster transitions tend to zero [Fig. 8(a)]. As discussed above, these transitions all have $\Delta k_c = \pm 3$, and so they have zero intensity in the absence of rotation–vibration interaction [5,26] but steal intensity from the fundamental vibrational transitions by a mechanism analogous to that discussed for H_3^+ in Section 14.1.14 of Ref. [5]. The intensity stealing is induced by rotation–vibration interaction between the vibrational ground state and excited vibrational states; the same interaction gives rise to centrifugal distortion effects. According to Ref. [32], the line strengths S_{if} for the $\Delta k_c = \pm 3$ transitions are given by

$$S_{if} = g_{ns} d_{03}^2 \frac{2J+1}{J(J+1)} (J \mp K_c)(J \pm K_c + 1)(J \mp K_c - 1) \times (J \pm K_c + 2)(J \mp K_c - 2)(J \pm K_c + 3), \tag{26}$$

where the dipole moment parameter d_{03} is an adjustable parameter. For K_c fixed, this expression increases with J

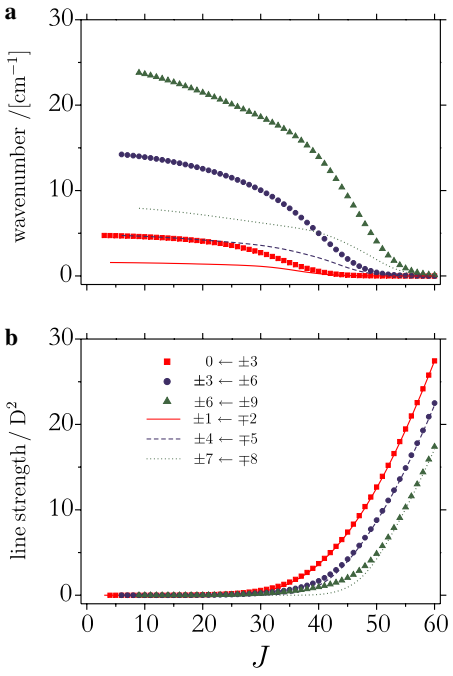

Fig. 8. (a) Transition wavenumbers and (b) line strengths S_{if} plotted against J for the intra-cluster transitions in the vibrational ground state of PH_3 defined in Fig. 7(A). The progressions are labeled by their respective values of $k'_c \leftarrow k''_c$.

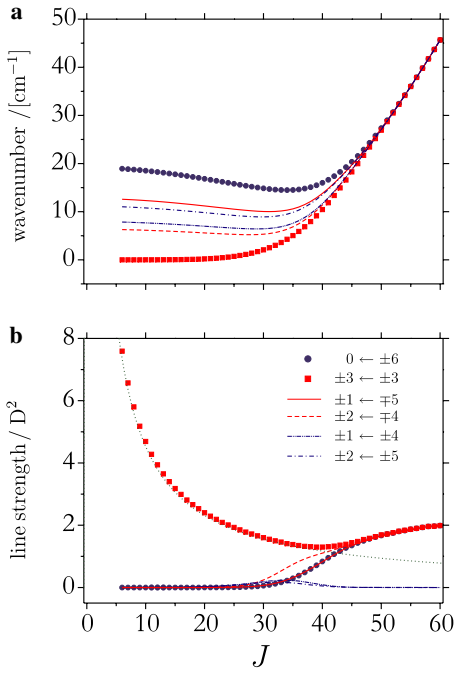

Fig. 9. (a) Transition wavenumbers and (b) line strengths S_{if} plotted against J for the inter-cluster transitions in the vibrational ground state of PH_3 defined in Fig. 7(B). The progressions are labeled by their respective values of $k'_c \leftarrow k''_c$. The dotted curve in (b) represents the function $23.7\ \mathrm{D}^2 \times (2J+1)/[J(J+1)]$; this is expression obtained in the customary theory for the line strengths of the $k_c = \pm 3 \leftarrow \pm 3$ transitions (see text).

and yields $S_{if} \sim J^5$ asymptotically for high J. This variation explains the moderate-J part (with $J < 40$) of Fig. 8(b). However, at $J > 40$, the line strengths exhibit an almost linear dependence on J, both for the $A_1 \leftrightarrow A_2$ and the $E \leftrightarrow E$ transitions. This effect reflects a qualitative change in the molecular motion, and indicates that for these highly excited states, corrections to Eq. (26) are necessary. A corresponding extension of the customary approximation will be discussed in detail below, where we take into account the dynamic effects explicitly by introducing a body-fixed xyz coordinate system suitable at very high J.

Fig. 9 shows the J-dependence of (a) the wavenumbers and (b) the line strengths for the $\Delta J = 0$ inter-cluster absorption transitions defined in Fig. 7(B). One progression comprises the transitions starting in the top state of the second cluster and ending in the bottom state of the first cluster. As discussed above, these transitions have $\Delta k_c = 0$; they have non-vanishing intensity also in the absence of rotation–vibration interaction. However, in the absence of rotation–vibration interaction they occur at zero wavenumber since the two states with $k_c = \pm 3$ are degenerate for a rigid PH_3 molecule. At low J, rotation–vibration interaction is weak and the $A_1 \leftrightarrow A_2$ transitions with $\Delta k_c = 0$ have appreciable intensity but a vanishingly low wavenumber as shown by the squares in the display (a) of Fig. 9. According to Ref. [32], the $\Delta k_c = 0$, $\Delta J = 0$ line strengths are given by

$$S_{if} = g_{ns} d_0^2 \frac{2J+1}{J(J+1)} K_c^2 \qquad (27)$$

(see also Eq. (12.31), in conjunction with Table 12.1, of Ref. [26]). In Eq. (27) d_0 is a dipole moment parameter. This S_{if} decreases with J and varies asymptotically as $2K_c^2/J$ for large J. The $K_c = 3 \leftarrow 3$ line strengths, shown by the squares in the display (b) of Fig. 9, indeed vary in this manner for low J. In Fig. 9(b) we show the function $23.7\ \mathrm{D}^2 \times (2J+1)/[J(J+1)]$ as a dotted line. The factor $g_{ns} d_0^2 K_c^2 = 23.7\ \mathrm{D}^2$ is computed using $d_0 = \mu_{fi} = 0.57395$ D (the experimental value of the ground state vibrational transition moment [25], see Table 3) and $g_{ns} = 8$. The other progression of $A_1 \leftrightarrow A_2$ transitions analyzed in the display (b) of Fig. 9 has $k_c = 0 \leftarrow \pm 6$ and therefore $\Delta k_c = \pm 6$ (shown by the circles); these transitions connect the bottom state of the second cluster with the top state of the first cluster. They gain intensity by rotation–vibration interaction and have zero intensity in the absence of this interaction. If we apply the contact transformation formalism [32] to these $k_c = 0 \leftarrow \pm 6$ transitions, we obtain $S_{if} \sim J^{11}$, which is in keeping with the variation exhibited by the circle transitions for $J < 40$ in Fig. 9(a). As the first and second clusters form for $J > 45$, the two progressions of $A_1 \leftrightarrow A_2$ transitions attain comparable wavenumbers and intensities, so that in Fig. 9(a), all the curves coalesce in this J region.

In Fig. 9, we also present the computed wavenumber and line-strength data for the $E \leftrightarrow E$ transitions defined in Fig. 7(B). The customary approach yields $S_{if} \sim J^5$ for $\Delta k_c = \pm 3$ transitions and $S_{if} \sim J^{11}$ for $\Delta k_c = \pm 6$ transitions. This explains, at least to some extent, the intensity variation for $J < 35$ in Fig. 9(a), shown by the solid,

dashed, and dot-dash lines. At higher J values, the $\Delta k_c = \pm 6$ transitions keep gaining intensity with increasing J in accordance with the J^{11}-variation, whereas the $\Delta k_c = \pm 3$ transitions lose intensity. The customary approach obviously does not explain the intensities of the $\Delta k_c = \pm 3$ transitions at very high J. As the first and second clusters form for $J > 45$, the two progressions of $E \leftrightarrow E$ transitions with $\Delta k_c = \pm 6$ merge, their wavenumbers and intensities become more or less identical, and identical to those of the corresponding $A_1 \leftrightarrow A_2$ transitions in Fig. 9(a). The two progressions of $E \leftrightarrow E$ transitions with $\Delta k_c = \pm 3$ follow the other progressions in wavenumber, but their intensities die out.

Finally, Fig. 10 shows the wavenumbers and line strengths of the $\Delta J = 1$, $\Delta k_c = 0$ inter-cluster transitions defined in Fig. 7(C). These transitions all have non-vanishing intensity in the absence of rotation–vibration interaction, and so they belong to the 'normal', allowed rotational spectrum of PH_3. This manifests itself in the fact that these lines are much stronger than the perturbation-allowed transitions considered in Fig. 9. In the absence of rotation–vibration interaction, Eq. (12.31), in conjunction with Table 12.1, of Ref. [26] give the line strengths of these $J \leftarrow J - 1$ transitions as

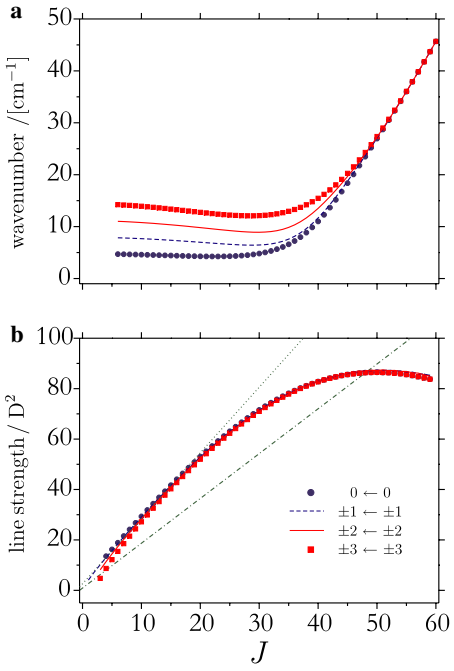

Fig. 10. (a) Transition wavenumbers and (b) line strengths S_{if} plotted against J for the inter-cluster transitions in the vibrational ground state of PH_3 defined in Fig. 7(C). The progressions are labeled by their respective values of $k_c' \leftarrow k_c''$. The dotted line in (b) represents the function $S_{if} = J \times 2.6\ \mathrm{D}^2$, the expression obtained in the customary theory for the line strengths of the inter-cluster transitions. The dot-dash line represents the function $S_{if} = J \times 1.8\ \mathrm{D}^2$, the expression obtained in the approximate theory that we develop for the high-J case (see text). In (b), the four progressions of calculated line strengths essentially coincide.

$$S_{if} = g_{\mathrm{ns}} d_0^2 \frac{J^2 - K_c^2}{J}. \tag{28}$$

For $K_c = 0$, this expression predicts the line strength to be proportional to J, and this is borne out by the results in Fig. 10(b) at moderate rotational excitation ($J < 40$). Using the experimental value of the vibrational transition moment d_0 in Eq. (28), we determine $S_{if} = 2.6\ \mathrm{D}^2 \times J$, which is shown in Fig. 10 as a dotted line. At very high J values the computed line strengths deviate from this straight line; at $J = 60$ they only have about half the value estimated from the linear dependence.

For all the 'cluster' transitions investigated here, we find that at $J > 35$, say, it becomes difficult to explain the variationally computed intensities in terms of the customary approach. This behavior is obviously caused by the six-fold cluster formation which sets in at these J values as discussed in Ref. [1]. During the cluster formation, the molecular rotation undergoes an important qualitative change in that the rotation axis changes; we can describe this by a change of the molecule-fixed axis system. In the classical picture the axis of rotation, associated with the topmost term values (with $K_c = 0, 1, 2, 3$) in each J manifold, gradually changes its orientation as the rotational excitation increases. At low J it lies in the plane perpendicular to the C_3 symmetry axis of the molecule, chosen as the molecule-fixed z axis, while at $J \gg 1$ it tends to coincide with one of the P–H bonds [1]. This process is illustrated in Fig. 5, where the rotational axis is labeled A. We aim at explaining the anomalous cluster intensities calculated variationally for $J > 35$ in terms of an alternative model, in which we change the molecule-fixed axis system so that one of the axes coincides with the rotational axis A. This new model involves four approximations:

(1) We consider PH_3 at the so-called strict local mode limit [33], which is based on the assumption that $m_P \gg m_H$ (m_P and m_H are the masses of the atoms P and H, respectively), that all bonds are exactly perpendicular to each other, and that all inter-mode interactions are negligible, including the vibration–vibration and rotation–vibration interactions. In this limit, the axis of stable rotation A coincides exactly with one of the P–H molecular bonds, say P–H_i (where the protons are labeled by $i = 1, 2, 3$) at $J \gg 1$ [1]. It is then natural to choose the new molecule-fixed axis system $x_i y_i z_i$ (see Fig. 5) in such a way that the z_i axis lies along the P–H_i bond. The other two axes x_i and y_i are then oriented along the two other bonds (which are exactly perpendicular to each other in the strict local mode limit) so that the $x_i y_i z_i$ axis system is right-handed.[2] The axes of the new $x_i y_i z_i$ axis system coincide with the unit vectors $\mathbf{e}_i$ defined for the MB system in Eq. (2).

[2] The origin of $x_i y_i z_i$ is at the molecular center of mass which, under the strict local mode conditions, coincides with the P nucleus.

(2) The rotational wavefunctions corresponding to the cluster states in the $x_iy_iz_i$ axis system are taken to be Wang-type rigid-rotor functions, and so the rotation–vibration wavefunctions are given by

$$\Psi_{v,J,K_i,\tau} = |v\rangle\tfrac{1}{\sqrt{2}}[|JK_i\rangle + (-1)^{\tau}|J-K_i\rangle], \tag{29}$$

where $\tau = 0, 1$, $K_i = |k_i|$ with k_i as the projection of the angular momentum onto the z_i axis in units of $\hbar$, and $|v\rangle$ is a purely vibrational function. In formulating Eq. (29) we have assumed that there is no vibration–rotation interaction so that K_i is a good quantum number.

(3) In expressing the dipole moment function $\bar{\boldsymbol{\mu}}$ in the new coordinate system $x_iy_iz_i$, we use the fact that the unit vectors $\mathbf{e}_i$ define the $x_iy_iz_i$ axes, and we obtain from Eq. (1)

$$\bar{\boldsymbol{\mu}} = \mu_0^{(\mathrm{LM})}(\mathbf{e}_1 + \mathbf{e}_2 + \mathbf{e}_3), \tag{30}$$

where the constant

$$\mu_0^{(\mathrm{LM})} = \bar{\mu}_1^{\mathrm{Bond}}(r_1 = r_2 = r_3 = r_e, \alpha_1 = \alpha_2 = \alpha_3 = 90^\circ) \tag{31}$$

is defined by the strict local mode limit. For $r_1 = r_2 = r_3$ and $\alpha_1 = \alpha_2 = \alpha_3$ we have $\bar{\mu}_1^{\mathrm{Bond}} = \bar{\mu}_2^{\mathrm{Bond}} = \bar{\mu}_3^{\mathrm{Bond}}$.

(4) The symmetrized cluster wavefunctions are linear combinations of the wavefunctions in Eq. (29). However, in determining line strengths we neglect contributions that involve wavefunctions from Eq. (29) with different values of i.

The line strength obtained with these approximations is given by Eq. (12.31) of Ref. [26]

$$S_{if} = g^{(i)}(2J+1)\left|\langle v|T^1_{\Delta k_i}(\bar{\mu})|v\rangle\right|^2 A(J, k_i, J', k_i') \tag{32}$$

where

$$g^{(i)} = \begin{cases} 2g_{\mathrm{ns}}^{(i)} & \text{for} \quad (K_i, K_i') = (0,1) \quad \text{or} \quad (1,0) \\ g_{\mathrm{ns}}^{(i)} & \text{otherwise} \end{cases}, \tag{33}$$

with $g_{\mathrm{ns}}^{(i)}$ as the nuclear spin statistical weight. Selection rules exist for the parameter τ in Eq. (29); Eq. (32) gives the line strengths of the transitions satisfying these selection rules. The irreducible tensor operators $T^1_{\Delta k_i}(\bar{\mu})$ (with $\Delta k_i = k_i' - k_i = 0, \pm 1$) in Eq. (32) are given by

$$T^1_{\pm 1}(\bar{\mu}) = \tfrac{1}{\sqrt{2}}(\mp\bar{\mu}_{x_i} - i\bar{\mu}_{y_i}) \tag{34}$$

and

$$T^1_0(\bar{\mu}) = \bar{\mu}_{z_i}, \tag{35}$$

where $(\bar{\mu}_{x_i}, \bar{\mu}_{y_i}, \bar{\mu}_{z_i})$ are the dipole moment components in the $x_iy_iz_i$ axis system, and the Hönl-London-factor $A(J, k_i, J', k_i')$ is defined in Table 12.1 of Ref. [26]. Strictly speaking, it makes no sense to define a spin statistical weight factor $g_{\mathrm{ns}}^{(i)}$ for the un-symmetrized wavefunctions from Eq. (29). However, these wavefunctions are all symmetrically equivalent, and as the six cluster states give rise to 32 total internal states [5] allowed by Fermi-Dirac statistics, it would seem reasonable to distribute these 32 spin states evenly over the six rotation–vibration states so that $g_{\mathrm{ns}}^{(i)} = 32/6 = 16/3$ in Eq. (32). This value is also obtained by formal application of the Landau-Lifshitz method for determining spin statistical weight factors (see Chapter 8 of Ref. [5]). It follows from Eqs. (30), (34), and (35) that

$$\left|\langle v|T^1_0(\bar{\mu})|v\rangle\right|^2 = \left|\langle v|T^1_{\pm 1}(\bar{\mu})|v\rangle\right|^2 = \left(\mu_0^{(\mathrm{LM})}\right)^2. \tag{36}$$

In the $x_iy_iz_i$ coordinate system the cluster states are characterized by $K_i = |k_i| \approx J$. When we insert the transition moment squares from Eq. (36) and the Hönl-London factors from Table 12.1 of Ref. [26] in Eq. (32) at the limit $J \gg 1$ and $K_i \to J$, we derive the line strengths

$$\begin{aligned} &(\mathrm{A})\Delta J = 0, \Delta K_i = 0 : S_{if} = g_{\mathrm{ns}}^{(i)}(\mu_0^{(\mathrm{LM})})^2(2J+1), \\ &(\mathrm{B})\Delta J = 0, \Delta K_i = 1 : S_{if} = g_{\mathrm{ns}}^{(i)}(\mu_0^{(\mathrm{LM})})^2(2J+1)/(J+1), \\ &(\mathrm{C})\Delta J = 1, \Delta K_i = 1 : S_{if} = g_{\mathrm{ns}}^{(i)}(\mu_0^{(\mathrm{LM})})^2(2J+1), \end{aligned} \tag{37}$$

where the labels (A), (B), (C) refer to Fig. 7.

Thus, for the intra-cluster transitions in Fig. 7(A), we obtain from Eq. (37) that the line strength varies linearly with J at high J. In terms of the wavefunctions given by Eq. (29), there are three symmetrically equivalent intra-cluster transitions, each with a line strength given by Expression (A) in Eq. (37). Fig. 7(A) shows, however, that in reality there are only two symmetry-allowed intra-cluster transitions with $K_c = 0 \leftarrow 3$ and $1 \leftarrow 2$, respectively. We combine the line strengths of the three 'un-symmetrized transitions' and distribute the total line strength evenly over the two symmetry-allowed ones. Each of these two transitions then gets a line strength of $3g_{\mathrm{ns}}^{(i)}(2J+1)(\mu_0^{(\mathrm{LM})})^2/2$. Since, in the strict local mode limit, the vector $\mathbf{e}_1 + \mathbf{e}_2 + \mathbf{e}_3$ has a length of $\sqrt{3}$, we can estimate the constant $\mu_0^{(\mathrm{LM})} \approx \mu_e/\sqrt{3} \approx 0.33$ D, where $\mu_e = 0.57736$ D is the equilibrium dipole moment. Thus Expression (A) in Eq. (37) gives $S_{if} = 3g_{\mathrm{ns}}^{(i)}(2J+1)(\mu_0^{(\mathrm{LM})})^2/2 \approx (2J+1) \times 0.9\ \mathrm{D}^2 \approx J \times 1.8\ \mathrm{D}^2$ for $J \gg 1$. The computed line strengths in Fig. 8(b) exhibit a linear dependence on J at high J, but the slopes of the lines are around 1 D^2 and thus significantly smaller than the predicted value of 1.8 D^2. We can take this as an indication that, as discussed also in Ref. [1], for PH_3 the local mode limit has not yet been reached at $J = 60$.

For the inter-cluster transitions in Fig. 7(B), the line strengths are predicted to reach a limiting value at high J. In this case there are six 'un-symmetrized transitions' that satisfy the selection rules on τ, and four symmetry-allowed ones. Thus we obtain a limiting value of $3g_{\mathrm{ns}}^{(i)}(\mu_0^{(\mathrm{LM})})^2 \approx 1.8\ \mathrm{D}^2$. We determine from Fig. 9 that for $J = 60$, the line strengths have values around 2 D^2, which is close to the limiting value that we estimate.

At low J, the line strengths of the $\Delta J = 1$ transitions in Fig. 7(C) vary approximately as $S_{if} = J \times 2.6\ \mathrm{D}^2$ [Eq. (28), dotted line in Fig. 10(b)]. Our approximate theory

(again with six 'un-symmetrized transitions' and four symmetry-allowed ones) predicts that at high J, they should also depend linearly on J, but with a smaller rate of increase: $S_{if} = J \times 1.8$ D^2 [dash-dotted line in Fig. 10(b)]. There is some indication of this behavior in Fig. 10(b): for J between 25 and 35, the calculated line strengths define an nearly straight line parallel to the dash-dot line. For higher J, however, the line strengths increase slower than $J \times 1.8$ D^2 and eventually start decreasing; the difference in centrifugal distortion effects when J is increased by one is probably important here.

A significant part of the discrepancies between the results of the approximate model and those of the variational calculation are caused by the fact that PH_3 is not at the strict local mode limit. In reality, the ratio m_P/m_H is not sufficiently large to put the center of mass at the P nucleus, and so as found in Ref. [1], at $J = 60$ (or even at $J = 80$) the axis of rotation does not coincide completely with a P–H bond. Test variational calculations with $m_P = 500$ u (so that we really have $m_P \gg m_H$), no coupling between the vibrational modes in the potential energy function, and 90° bond angles give a significantly better agreement with the results of the approximate model than that obtained with the calculations reported here for the 'real existing' PH_3 molecule.

We conclude that for PH_3, the cluster-formation (or localization) effects appearing in the rotational energy level spectrum cause very significant qualitative changes to the cluster-transition line strength values at high J.

6. Summary and conclusion

We have computed *ab initio*, at the CCSD(T)/aug-cc-pVTZ level of theory, the dipole moment for the electronic ground state of PH_3 at 10 080 unique molecular geometries covering a large volume of vibrational coordinate space. A six-dimensional, Molecular-Bond representation of the dipole moment surface has been obtained by fitting suitable parameterized analytical functions through the *ab initio* points; see Eqs. (1)–(10). We have used this analytical DMS to calculate vibrational transition moments for selected vibrational bands. The theoretical transition moments were found to reproduce very satisfactorily the available experimentally determined values. By means of recently developed computational methods for calculating rotation–vibration energies and intensities for isolated electronic states of XY_3 pyramidal molecules [7,8], we have simulated several rotation–vibration bands of PH_3; the wavenumbers and intensities determined for the individual transitions in these bands are also in very satisfactory agreement with experimental data. For example, for the ν_2/ν_4 fundamental bands, whose upper states interact, we reproduce, with our purely *ab initio* DMS, 955 observed [27] intensity values with an average absolute percentage deviation of 8.7% (and a root-mean-square deviation of 0.94 cm^{-1} for the transition wavenumbers). The deviation of 8.7% is larger than the 1.5% and 2.1% obtained by Brown et al. [27] in a least-squares fitting to the experimental intensity values for the ν_2 and ν_4 bands, respectively, but we find the relatively small difference encouraging. It shows that *ab initio* calculations are reaching a level of accuracy where they can provide intensity data of sufficient quality to compete with the very often exceedingly difficult experimental intensity measurements (see also Ref. [34]).

Using our theoretical model for the rotation–vibration motion of an XY_3 molecule [6–9,35], which is based on the Hougen–Bunker–Johns approach [5,10], we can calculate the energies and wavefunctions of highly excited rotational states [1] and the line strengths of the transitions that involve these states. We have already shown [1] that in the vibrational ground state of PH_3, at high rotational excitations the energy levels cluster to produce six-fold near-degenerate states, and in the present work we have studied the line strengths of the transitions between these states. In particular, the so-called intra-cluster transitions (Fig. 8) have wavenumbers that tend to zero as J increases. That is, with increasing J these transitions move through the THz, mm-wave, and microwave regions where spectroscopy with ultra-high resolution and ultra-high sensitivity is possible. Thus, one could imagine that the cluster states could be characterized by such spectroscopic methods as it happened for the analogous cluster states in H_2Se [36]. The investigation of these states could help elucidate the phenomenon of rotationally induced chirality discussed for triatomic molecules by Bunker and Jensen [37]. The problem is, however, that the energy clusters are found at very high term values (see Table 5) so that a relatively high temperature is needed to populate the initial states of the intra-cluster transitions. Even then, the transitions will be weak and require experiments at high PH_3 pressure to be detected. The unfortunate fact that PH_3 is both poisonous and volatile may dampen the enthusiasm for undertaking experimental investigations of the interesting cluster phenomenon in this molecule.

After we had submitted the initial version of the present work, Butler et al. [38] reported new measurements of phosphine intensities in the 2.8–3.7 μm region. They did not, however, use the experimental intensity values to determine vibrational transition moments that we can compare with our theoretical results. Instead they list, for a number of bands, 'sum intensities' (i.e., sums of the intensities of observed/assigned transitions in a given band) which provide rough measures of the total band intensity. Sum intensities obtained from our simulated spectra show broad agreement with the new experimental values so that this comparison provides further validation of our new *ab initio* dipole moment surface for the electronic ground state of PH_3.

Acknowledgments

This work was supported by the European Commission through Contract No. MRTN-CT-2004-512202 "Quantitative Spectroscopy for Atmospheric and Astrophysical Re-

search.'' The work of P.J. is supported in part by the Deutsche Forschungsgemeinschaft and the Fonds der chemischen Industrie.

References

[1] S.N. Yurchenko, W. Thiel, S. Patchkovskii, P. Jensen, Phys. Chem. Chem. Phys. 7 (2005) 573–582.
[2] S.N. Yurchenko, M. Carvajal, P. Jensen, F. Herregodts, T.R. Huet, Chem. Phys. 290 (2003) 59–67.
[3] D. Wang, Q. Shi, Q.-S. Zhu, J. Chem. Phys. 112 (2000) 9624–9631.
[4] P. Jensen, G. Osmann, I.N. Kozin, in: D. Papoušek (Ed.), Vibration–Rotational Spectroscopy and Molecular Dynamics, World Scientific, Singapore, 1997.
[5] P.R. Bunker, P. Jensen, Molecular Symmetry and Spectroscopy, second ed., NRC Research Press, Ottawa, 1998.
[6] H. Lin, W. Thiel, S.N. Yurchenko, M. Carvajal, P. Jensen, J. Chem. Phys. 117 (2002) 11265–11276.
[7] S.N. Yurchenko, M. Carvajal, P. Jensen, H. Lin, J.J. Zheng, W. Thiel, Mol. Phys. 103 (2005) 359–378.
[8] S.N. Yurchenko, M. Carvajal, W. Thiel, H. Lin, P. Jensen, Adv. Quant. Chem. 48 (2005) 209–238.
[9] S.N. Yurchenko, M. Carvajal, H. Lin, J.J. Zheng, W. Thiel, P. Jensen, J. Chem. Phys. 122 (2005) 104317.
[10] J.T. Hougen, P.R. Bunker, J.W.C. Johns, J. Mol. Spectrosc. 34 (1970) 136–172.
[11] S.-G. He, JJ. Zheng, S.-M. Hu, H. Lin, Y. Ding, X.-H. Wang, Q.-S. Zhu, J. Chem. Phys. 114 (2001) 7018–7026.
[12] A.D. Becke, J. Chem. Phys. 98 (1993) 5648–5652.
[13] C. Lee, W. Yang, K.G. Parr, Phys. Rev. B37 (1988) 785–789.
[14] K. Raghavachari, G.W. Trucks, J. Chem. Phys. 91 (1989) 1062–1065.
[15] MOLPRO, Version 2002.3 and 2002.6, a package of ab initio programs written by H.-J. Werner, P.J. Knowles, with contributions from R.D. Amos, A. Bernhardsson, A. Berning et al.
[16] C. Hampel, K. Peterson, H.-J. Werner, Chem. Phys. Lett. 190 (1992) 1–12, and references therein. The program to compute the perturbative triples corrections has been developed by M.J.O. Deegan, P.J. Knowles, Chem. Phys. Lett. 227 (1994) 321–326.
[17] G.D. Purvis, R.J. Bartlett, J. Chem. Phys. 76 (1982) 1910–1918.
[18] M. Urban, J. Noga, S.J. Cole, R.J. Bartlett, J. Chem. Phys. 83 (1985) 4041–4046.
[19] K. Raghavachari, G.W. Trucks, J.A. Pople, M. Head-Gordon, Chem. Phys. Lett. 157 (1989) 479–483.
[20] T.H. Dunning, J. Chem. Phys. 90 (1989) 1007–1023.
[21] D.E. Woon, T.H. Dunning, J. Chem. Phys. 98 (1993) 1358–1371.
[22] R. Marquardt, M. Quack, I. Thanopulos, D. Luckhaus, J. Chem. Phys. 119 (2003) 10724–10732.
[23] D.A. Helms, W. Gordy, J. Mol. Spectrosc. 66 (1977) 206–218.
[24] K. Kijima, T. Tanaka, J. Mol. Spectrosc. 89 (1981) 62–75.
[25] P.B. Davies, R.M. Neumann, S.C. Wofsy, W. Klemperer, J. Chem. Phys. 55 (1971) 3564–3568.
[26] P.R. Bunker, P. Jensen, Fundamentals of Molecular Symmetry, IOP Publishing, Bristol, 2004.
[27] L.R. Brown, R.L. Sams, I. Kleiner, C. Cottaz, L. Sagui, J. Mol. Spectrosc. 215 (2002) 178–203.
[28] G. Tarrago, N. Lacome, A. Lèvy, G. Guelachvili, B. Bèzard, P. Drossart, J. Mol. Spectrosc. 154 (1992) 30–42.
[29] D. Papoušek, M.R. Aliev, Molecular Vibrational/Rotational Spectra, Elsevier, Amsterdam, 1982.
[30] M.R. Aliev, J.K.G. Watson, Higher-order effects in the vibration–rotation spectra of semirigid molecules, in: K. Narahari Rao (Ed.), Molecular Spectroscopy: Modern Research, vol. III, Academic Press, New York, 1985.
[31] K. Sarka, J. Demaison, Perturbation theory, effective Hamiltonians and force constants, in: P. Jensen, P.R. Bunker (Eds.), Computational Molecular Spectroscopy, Wiley, Chichester, 2000.
[32] G. Tarrago, O.N. Ulenikov, G. Poussigue, J. Phys. 45 (1984) 1429–1447.
[33] L. Halonen, A.G. Robiette, J. Chem. Phys. 84 (1986) 6861–6871.
[34] S.N. Yurchenko, J. Zheng, W. Thiel, M. Carvajal, H. Lin, Per Jensen, Theoretical quantitative spectroscopy: Computer simulation of molecular spectra, in: N. Ben Sari Zizi, J. Demaison, A. Perrin (Eds.), Remote Sensing of the Atmosphere for Environmental Security, Proceedings of the NATO Advanced Research Workshop in Rabat, 16–19 November 2005, Morocco, Springer, Dordrecht, 2006, in press.
[35] S.N. Yurchenko, H. Lin, J.J. Zheng, P. Jensen, W. Thiel, J. Chem. Phys. 123 (2005) 134308.
[36] I.N. Kozin, S.P. Belov, O.L. Polyanski, M.Yu. Tretyakov, J. Mol. Spectrosc. 152 (1992) 13–28.
[37] P.R. Bunker, P. Jensen, J. Mol. Spectrosc. 228 (2004) 640–644.
[38] R.A.H. Butler, L. Sagui, I. Kleiner, L.R. Brown, J. Mol. Spectrosc. doi:10.1016/j.jms.2006.04.021.